Latin American Journal of Solids and Structures
www.lajss.org

Developing and Multi-Objective Optimization of a Combined Energy Absorber Structure Using Polynomial Neural Networks and Evolutionary Algorithms

Abstract

In this study a newly developed thin-walled structure with the combination of circular and square sections is investigated in term of crashworthiness. The results of the experimental tests are utilized to validate the Abaqus/Explicit^{TM} finite element simulations and analysis of the crush phenomenon. Three polynomial meta-models based on the evolved group method of data handling (GMDH) neural networks are employed to simply represent the specific energy absorption (SEA), the initial peak crushing load (P1) and the secondary peak crushing load (P2) with respect to the geometrical variables. The training and testing data are extracted from the finite element analysis. The modified genetic algorithm NSGA-II, is used in multi-objective optimisation of the specific energy absorption, primary and secondary peak crushing load according to the geometrical variables. Finally, in each optimisation process, the optimal section energy absorptions are compared with the results of the finite element analysis. The nearest to ideal point and TOPSIS optimisation methods are applied to choose the optimal points.

Keywords

Combined energy absorber, Multi-objective optimization, GMDH neural network,Modified genetic algorithm NSGA-II, Pareto curves.

Amir Najibi [a]
Mohammad Hassan Shojaeefard [b]
Mohsen Yeganeh [c]

[a] Faculty of Mechanical Engineering, Semnan University, Campus 1, Semnan, Iran, P.O. Box: 35131-19111.
E-mail: a.najibi@semnan.ac.ir
[b] School of Mechanical Engineering, Iran University of Science& Technology, Iran.
E-mail: mhshf@iust.ac.ir
[c] School of Automotive Engineering, Iran University of Science& Technology, Iran.
E-mail:mohsenyeganeh@gmail.com

http://dx.doi.org/10.1590/1679-78252797

Received 15.01.2016
In revised form 29.06.2016
Accepted 04.07.2016
Available online 29.08.2016

1 INTRODUCTION

For modelling a system, it is essential to evaluate precisely the relations between input and output data in a simple manner (Åström and Eykhoff, 1971). Given that neural network and genetic algorithm have the ability to model the complicated systems (Sanchez et al., 1997), many attempts have been made to introduce evolutionary methods (Farlow, 1984). For the first time Ivakhnenko

utilized GMDH (Group Modelling and Data Handling) method which is applicable for modelling the systems with several inputs and one output (Ivakhnenko, 1971). In fact, the main idea of the GMDH is to develop a function according to second order transfer function and recently genetic algorithm in conjunction with GMDH neural network has been performed for optimum connection between variables (Atashkari et al., 2007).

Mamalis and Johnson investigated crushing of aluminium tubes and Frusta under static pressure (Mamalis and Johnson, 1983; Mamalis et al., 1986). Mainly aiming to obtain a detailed experimental study of the failure modes, they presented a theoretical model for predicting the energy and the average load of plastic buckling in the crushing of cylindrical thin walls and Frusta in the axial symmetric deformation mode. Qi et al. has investigated the crash behaviour of the four types of axisymmetric thin-walled square (ATS) tubes (Qi et al., 2012). It has been found that the multi-cell tapered (MCT) tube has the best crashworthiness performance under oblique impact regarding to both the specific energy absorption (SEA) and peak crushing force (PCF). The energy absorption of empty and foam-filled tubes under oblique loading with different loading angles and geometry parameters has been carried out by Li et al. (Li et al., 2012). It has been shown that the energy-absorbing effectiveness factors of the circular tube structures with aluminium foam core are significantly higher than those of the empty tubes, and the energy absorption capacity of the foam-filled double tubes is better than that of the empty and foam-filled single tubes. Bi et al. has optimized single and triple-cell hexagonal columns filled with aluminium foams for maximum specific energy (Bi et al., 2010). The results showed that foam-filled columns had significantly larger crushing forces than those of non-filled columns due to interactions between the tube and foam. The optimization results further suggested that the SEA tend to favour slender and thick columns with a moderate foam density for both single and triple-cell columns. Yin et al.'s have investigated two kinds of functionally lateral graded foam-filled tubes (FLGFTs), and the numerical results indicated that each of those two kinds of FLGFTs demonstrates higher energy absorption capacity than the ordinary uniform foam-filled tube (UFT) with the same weight (Yin et al., 2013). A comprehensive experimental investigation on the response of the composite sandwich structures exposed to quasi-static compression has been carried out by Tarlochan and Ramesh, in which average crushing force and crush force efficiency of various types of composite sandwich structures were investigated in a series of edgewise axial compression tests (Tarlochan and Ramesh, 2012). Four distinct modes of failure were observed and recorded, among which the primary mode of observed failure was progressive crushing with high energy absorption capability. Ghafari and Ghasemnejad studied the effects of stitching on the energy absorption and crashworthiness behaviour of the composite box structures (Ghafari-Namini and Ghasemnejad, 2012). It was found that the stitched composite boxes which show higher fracture toughness in Mode-I delamination tests, are not necessarily able to absorb more crushing energy in comparison with non-stitched composite boxes. Qureshi and Bertocchi have proposed a new automotive box-beam crash absorber design with sinusoidal patterns embedded on the beam surfaces. Six different types of surface patterns were initially put forward and a total of 43 samples have been simulated using the commercial pre-processor Hyper Crash^{TM} and the commercial explicit FEM solver RADIOSS^{TM}. A maximum increase of 42 percent in the amount of total energy absorption and an increase in the energy efficiency factor from 1.08 to 1.54 were observed moving from the reference model to the best design so far (Qureshi and Bertocchi, 2012).

The bending crashworthiness of empty and foam-filled thin-walled circular tubes has been investigated through dynamic three-point bending experiments by Li et. al. Three types of tubular structures have been tested and due to their high dynamic bending resistance and energy-absorbing effectiveness, foam-filled double circular tube structures have been recommended as crashworthy structures (Li et al., 2013). Costas et al. have performed surrogate-based multi-objective optimization techniques to a crashworthiness problem in which the impact performance of a frontal crash absorber made of steel and a glass-fiber reinforced polyamide has been optimized. The Specific Energy Absorption (SEA) and the Load Ratio (LR), whose responses were approximated by multiple types of surrogate models, have been considered as contrasting objective functions. The results show improvements in both functions by almost 50% compared to the original design (Costas et al., 2014). Multi-cell square tubes under dynamic oblique impact loading have been studied by Trong Nhan Tran et. al. The theoretical predictions of mean crushing force mean horizontal force, and mean bending moment were proposed based on a Simplified Super Folding Element theory. The optimal configurations of multi-cell tubes have been analyzed under axial and more than one oblique impact loadings. The results showed that the FE numerical results agreed well with the theoretical predictions (Tran et al., 2014). Shojaeefard et. al. have been performed Quasi-static experimental and nonlinear finite element analyses to compare the energy absorption and initial peak load of combined circular and square sections with those of regular circular and square sections. Results showed that the specific energy absorption capability of the combined tube is significantly higher than that of the square tube and is close to that of the circular tube. Moreover, the initial peak load of combined tube is significantly lower than that of the circular tube and somewhat lower than that of the square tube (Shojaeefard et al., 2014). Baroutaji et al.has studied the energy absorption behavior and crashworthiness optimization of short length circular tubes under quasi-static lateral loading. Response surface methodology (RSM) for design of experiments (DOE) has been utilized in conjunction with finite element modelling to evaluate systematically the effects of geometrical parameters on the energy absorption responses of laterally crushed circular tubes. The approach of multi-objective optimization design (MOD) has been employed to find the optimal configuration of the proposed energy absorption structures (Baroutaji et al., 2015). Djamaluddin et. al. have been presented the multi-objective optimization of the foam-filled double circular tubes under pure axial and oblique impact loadings. So different configurations of structures, such as empty double tube (EET), foam filled empty double tube (FET) and foam filled foam filled double tube (FFT), have been identified for their crashworthiness performance indicators. The results showed that the optimal FFT had better crashworthiness performance than the others under pure axial loading (Djamaluddin et al., 2015). Bi-tubal circular energy absorbers consist of two AL-6063-O tubes with unequal diameters placed coaxially and compressed under quasi-static axial load have been studied experimentally by Sharifi et al. In order to reduce the high value of peak load induced in the bi-tubal absorbers, two worthwhile solutions are proposed. The first one is to use two tubes with different lengths and the other one is to cut groove at the end portion of one of the tubes (Sharifi et al., 2015).

This paper aims to optimize a new combined energy absorber (square-circular section) for the improvement of its crashworthiness characteristics. This combination is not presented in any other literature until now. The idea comes from the superior capabilities of energy absorption of the thin-

walled square and circular sections. The square sections though with the lower energy absorption and initial peak load in comparison with the circular ones are however used in automotive industries as front rail to absorb the crash energy. Nowadays, with tougher safety standards the development of an energy absorber with high capability of energy absorption beside low initial peak load is inevitable. When the square and circular sections designate in series form, the new configuration shows the superiorities over both square and circular sections. It also gives the designer more functionality to manage the energy absorption of each part of vehicle in collision. Higher energy absorption with lower initial load peaks can be achieved through optimizing the geometry variables of these structures. For example, the pedestrian–vehicle collision needs softer front structure which is withstanding the high speed collisions.

In this paper the newly developed combined energy absorber structures with the combination of circular and square sections are investigated in terms of crashworthiness. Experimental tests have been firstly performed and then the result of the Abaqus/Explicit^{TM} finite element simulation has been validated with the experimental test results. Four polynomial meta-models based on the evolved group method of data handling (GMDH) neural networks have been employed to simply represent the specific energy absorption (SEA), the initial peak crushing load (P1) and the secondary peak crushing load (P2) with respect to geometrical variables. Comparing the results of the models with the simulation ones indicates that this model has been successfully developed in the mentioned processes. The modified genetic algorithm NSGA-II and Pareto curves have utilized for the multi-objective optimization of the specific energy absorption primary and secondary peak crushing load. At the end of each optimization process by using the nearest to ideal point and TOPSIS, optimal sections have been selected. The obtained optimal points have been re-evaluated with the Abaqus/Explicit^{TM} finite element software. The very close agreement of these results with those of numerical results using the GMDH model demonstrates the effectiveness of our approach in this paper.

2 COMBINED ENERGY ABSORBER

Combined energy absorbers are composed of square and circular section tubes in series form. Circular crash boxes always have higher energy absorption than the square ones, but the initial peak in the circular crash boxes is much higher than the square ones. Since higher initial peaks lead to severe injuries for the automotive passengers, the circular crash boxes are not utilized in automotive structure for the aim of the energy absorption (Kiasat and Najibi, 2008). To overcome this drawback the combined energy absorber is proposed for the first time. This proposed structure not only has the lower initial peak but also manifests high energy absorption like the circular crash boxes. The Geometry variables are b, R, l and t which stand for square section width, circle section radius, length of square section and thickness of the structures respectively. The total length of the structures is constrained to 588mm and both of the circular and square tubes are made of steel.

The combined energy absorber in comparison with the square energy absorber with the same geometry (e.g., the width of square tube equal to 90mm; the length and thickness equal to 588mm and 2mm respectively) has about 22% more energy absorption, while their initial peak loads are the same. The combined energy absorber in comparison with the circular energy absorber in which the circle section radius is 55 mm and the length and thickness is equal to 588mm and 2mm respective-

ly, has about 33% less initial peak load, while their energy absorptions are the same (Figures 1 and 2).

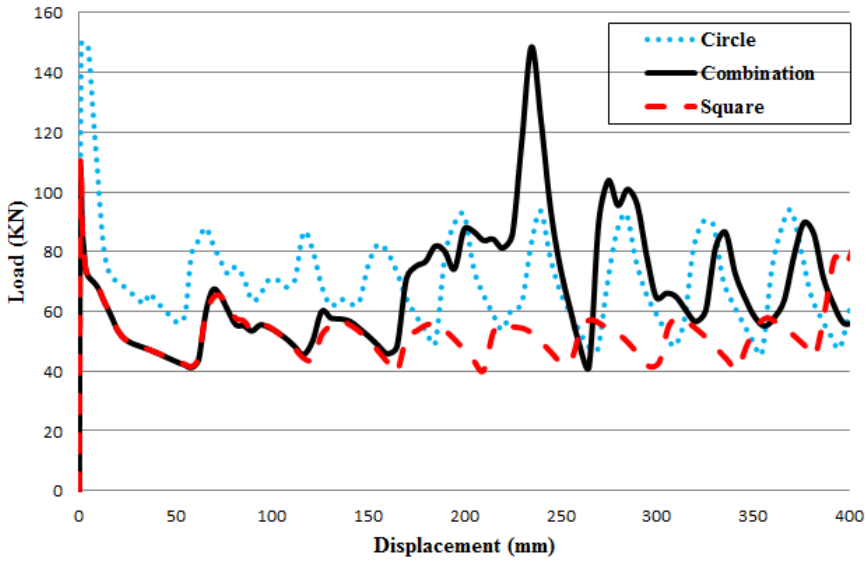


Figure 1: Comparison of the numerical force–displacement diagrams of square, circular and combined sections.

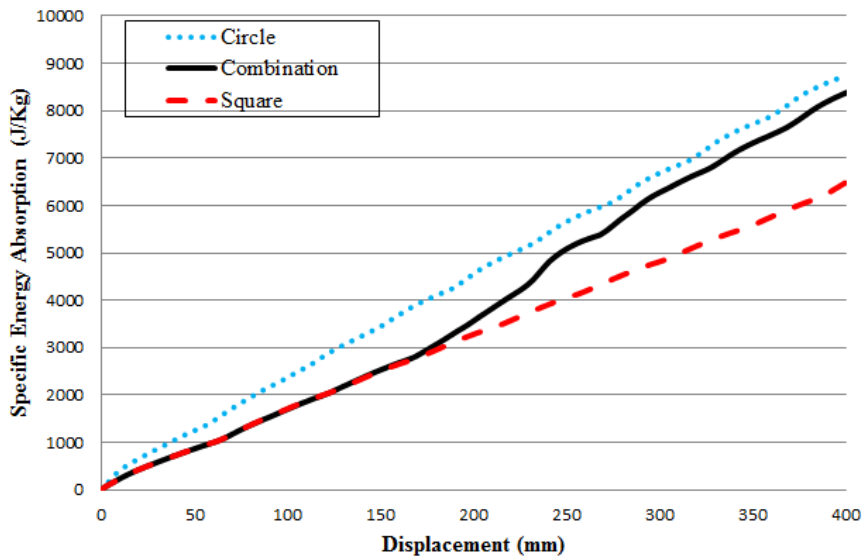


Figure 2: Comparison of the numerical energy–displacement diagrams of square, circular and combined sections.

3 EXPERIMENTAL TESTS

For the experimental test it is needed to fix the crash boxes between the upper and lower parts of the pressure machine. The bottom and top of the crash boxes must be clamped; therefore, the

square fixing plates with thickness of 15mm and 150*150mm were developed to clamp the 6 degrees of the freedom of the crash box ends. There are 3 types of these fixing plates: 1) the first type on the plate is a square slot with thickness of 6 mm was made for square section; 2) the Second type is a circular slot with thickness of 6mm to clamp the circular section; and 3) the third type is designed to keep the circular and square sections clamped to each other's. Note that this last type of fixing plates is embedded between those sections to keep the continuity of the combined section.

Four screws have been employed in every plate for avoiding the tube ends movements. Quasi-static tests have been performed by INSTRON^{TM} pressure machine with a load capacity of 30000 kg in speed of 10 mm/min and total displacement of 382 mm. Three experimental tests have been performed for the combined energy absorber and the average results were considered for load-displacement graphs. In the experimental tests the thickness of each tube is 2mm. The length of the combined energy absorber is 588mm which is close to the automotive front rail. Considering the equal length for each section the length for each section would be 294mm, and for reaching the equal mass of each section the square section width would be equal to 90 mm and the circular section radius would be equal to 55mm. To determine the exact behaviour of the combined energy absorber by changing the four design variables like b (The square section width between 60 and 150 mm), t (the thickness of tube between 1 and 2 mm), L (The length of square section between 60 and 530 mm) and R (The circle section radius between 43 and 83 mm) with a constant total length of structure equal to 588 mm, it is needed to do a large number of numerical tests. For this purpose, 207 numerical tests were conducted with the ABAQUS software in our research.

4 FINITE-ELEMENT SIMULATION AND VALIDATION

Validated numerical simulation would be helpful since experimental tests are usually time and cost consuming and sometimes impossible. For the goal of this study a lot of tests need for training the neural network, and simulation analyses would thus be unenviable.

As mentioned above the experimental quasi-static tests have been carried out and the load-displacement and energy-displacement response curves have been extracted to validate the numerical simulation. The numerical quasi-static crushing study has been performed using commercial software ABAQUS/Explicit^{TM}.

Sudden movements cause stress waves propagation which can induce noisy or inaccurate solution. Therefore, it is needed to apply loading as smooth as possible. To ensure the accuracy of the quasi-static analysis, the loading rate was ramped smoothly to the applied velocity during first time increments and the applied velocity was also artificially raised to reduce the required solution time. A typical smooth loading curve is shown in Figure3, where the initial velocity and initial slope of this curve which is equal to initial acceleration are clearly zero. This ensures that loading takes place gradually and unnecessary dynamic effects would be avoided.

In the quasi-static simulation, the velocity of the material is considered very small and so that the inertial forces are negligible. Therefore, internal energy is nearly equal to the work applied by the external forces while the kinetic energy is small and should not exceed a small fraction of internal energy.

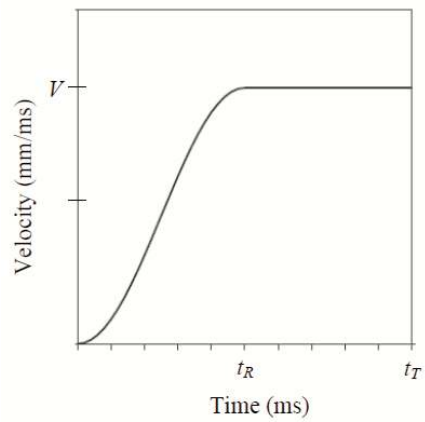


Figure 3: Velocity-Time history for the moving rigid body used in the quasi-static simulation (Shojaeefard et al., 2014).

The tubes which are made of steel modelled with elastic and plastic properties. The material properties of those tubes were calculated using Equations (1) and (2), and the stress–strain curves obtained from uniaxial tensile tests (Reid et al., 1986) and (Karagiozova et al., 2000).

$$\sigma_{True} = \sigma_{Eng}(1 + \varepsilon_{Eng}) \tag{1}$$

$$\varepsilon_{Plastic} = Ln(1 + \varepsilon_{Eng}) - \sigma_{True}/E \tag{2}$$

where, σ_{Eng} and σ_{True} are the engineering and true stresses, respectively, while ε_{Eng} and $\varepsilon_{Plastic}$ are the engineering and plastic strains, respectively.

The finite element models of the combined energy absorber were developed in the nonlinear finite element software environment (Abaqus/Explicit^{TM}). In the simulation 4-node, doubly curved thin shell elements, *S4R*, which are suitable for large strain analysis (Figure4) have been utilized. The element size is taken small enough in which the difference between structure energy absorptions with this element size and the previously taken element size is less than 0.5%. Thus, the final element size applied in these simulations is 6 mm. In order to simulate crushing, five integration points were selected through the shell thickness.

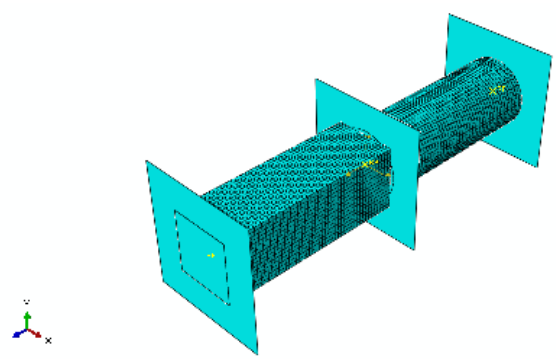


Figure 4: The finite element model of the combined energy absorber.

In this paper, the density of the steel tubes is 7800 Kg/m^3 and the module of elasticity of them is 207 GPa. The elastic-plastic properties of steel tubes which have been achieved from the conventional experimental tensile test have been depicted in Figure 5.

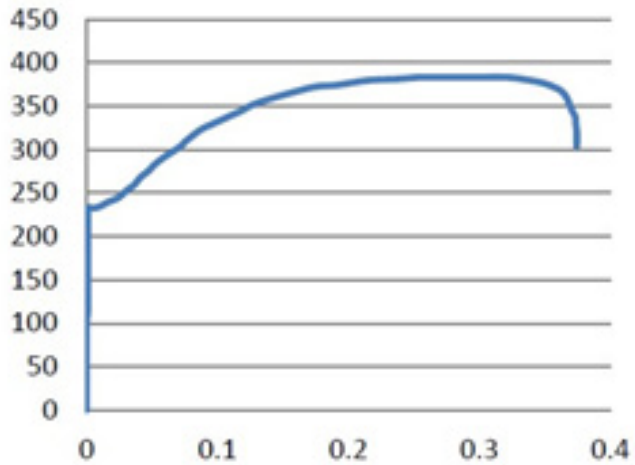


Figure 5: The stress-strain curve.

The movable flat plate which was a member of fixture at the top in the experiments has been modelled as a discrete rigid surface. This surface has been considered free just in the vertical direction. The contact between top, bottom and middle of the plate is fully clamped and in the numerical simulation "tie" interaction has been applied. Moreover, the all degrees of the freedom of the lower end of the tube have been constrained to model the connection between the tube and the lower fixture and the velocity has been applied to the tube via the rigid surface.

In order to reduce the time needed to analyze in the software, the velocity of the rigid surface was artificially speeded up to 2 m/s. Moreover, the applied velocity has controlled using the AMPLITUDE option and the SMOOTH STEP sub option in ABAQUSE/Explicit^{TM} to ensure an accurate quasi-static analysis.

According to Figure 6 it is clear that the collapse mode in the square section of the combined energy absorber follows a symmetric deformation, while in the circular section it is symmetric first and then develops into the Diamond type deformation mode in both experimental and numerical simulation. It can be obviously seen that in Figure 7, there are two peaks in the load-displacement curves of the combined energy absorber. The first peak is called the initial peak and occurs because of the crushing of the square section. The second peak comes from the crushing of the circular section. When crushing occurs at first, the square section is going to crumple because it requires less initial crushing load. Then the circular section crushing begins, leading to the emergence of the second peak. If the impact severity is low, only the square section will collapse. In the severe crushes the circular section will incorporate in the crush after the square one. The summary results of the experimental and simulation results are given in Table 1.

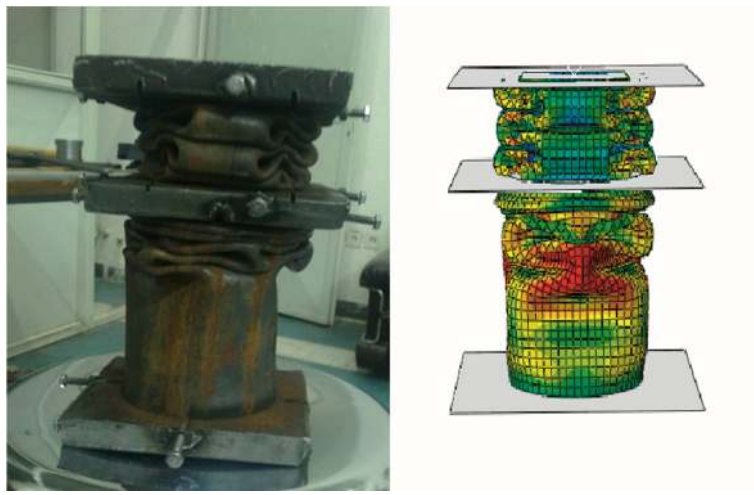


Figure 6: Comparison of Final deformed profiles of combination absorber under the experimental and numerical tests.

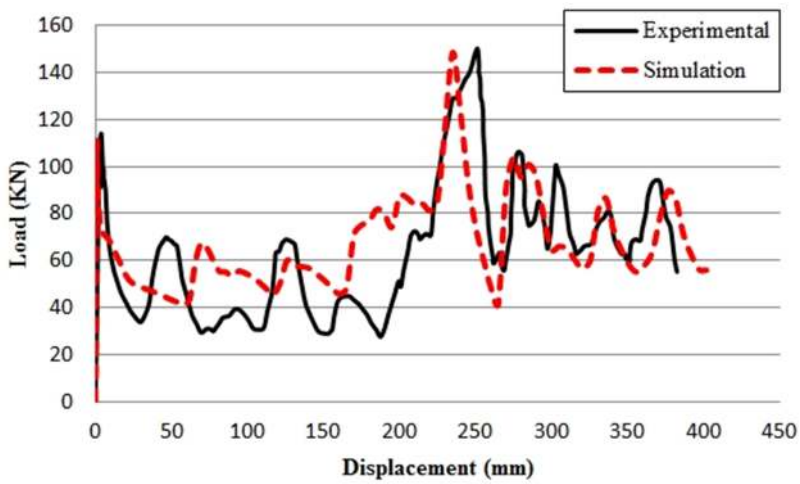


Figure 7: Quasi-static load-displacement histories of combined energy absorber.

The small difference between numerical and experimental results indicates the accuracy of the numerical simulation. 207 various finite-element analyses considering the variations of design variables were performed under the same load and boundary conditions. In this way, the square section width b is changed between 60 and 150 mm, whilst the thickness of tube t varies between 1 and 2 mm, The length of square section l changed between 60 and 530 mm, and the circle section radius R changed between 43 and 83 mm. Table 2 depicts that the values of some input data and the computed values of the absorbed energy, specific energy absorption, initial and secondary peaks crushing load as output data. In the numerical study, the energy absorption during deformation of the combined energy absorbers has been computed at the time when the end displacement reached 382 mm. The results obtained in such finite-element analysis can now be used to build the equations (7,

8 and 9) of both the energy absorption capacity and the maximum crushing force for those different 207 models using GMDH-type polynomial neural networks. Such meta-models will be then used for the multi-objective optimization of the combined energy absorber. The solutions which have been calculated by means of the approach of this paper exhibit some important trade-offs among those objective functions which can be simply used by a designer to optimally compromise among the obtained solutions.

Combination Section	Absorbed Energy (J)	Initial Peak (KN)	Secondary Peak (KN)
Experiment	25402	114.20	150.80
Simulation	25963	111.05	148.52
Difference With Experiment (%)	+ 2.2	- 2.7	- 1.5

Table 1: Summary of the quasi-static axial loading tests.

5 MODELLING WITH THE GMDH-TYPE NEURAL NETWORK

GMDH algorithm represents a model as a set of neurons in which different pairs of them in each layer are connected through a quadratic polynomial and thus reproduce new neurons in the next layer. Such representation can be used in modelling to find a function between inputs and outputs. The formal definition of the identification problem is to find a function $\hat{f}$ so that it can approximate the actual one , f , with the purpose of predicting output "*y*" for a given input vector $X = (x1, x2, x3, \ldots, xn)$ as close as possible to its actual output "*y*". Therefore, for multi-input single-output data pairs we have:

$$y_i = f(x_{i1}, x_{i2}, x_{i3}, ..., x_{in}) \quad i = 1,2,...,n \tag{3}$$

Input Data				Output Data			
$R(mm)$	$l(mm)$	$b(mm)$	$t(mm)$	$E(J)$	$SEA(J/Kg)$	$P_1(KN)$	$P_2(KN)$
43	294	90	1	7430	5148.448	35.96	52.24
63	294	100	1	8823	4839.683	36.90	80.32
83	294	110	1	9695	4400.910	38.09	99.22
56	117.6	100	1	9299	5582.368	39.65	71.88
56	352.8	110	1	8118	4385.569	36.47	68.99
51	294	90	1.5	15604	6679.346	70.85	100.84
83	294	110	1.5	18196	5509.008	76.74	156.51
55.5	294	80	1.5	16696	7272.338	71.05	111.73
55.5	235.2	100	1.5	16427	6459.450	71.04	101.66
55.5	529.2	110	1.5	11882	4054.852	72.62	58.47
55	294	70	2	26782	9360.198	118.00	146.87
71	294	100	2	28126	7262.619	114.53	187.34
83	294	110	2	29757	6759.928	116.68	207.83
55	352.8	100	2	25792	7479.295	115.27	147.54
55	352.8	110	2	25334	6905.631	125.00	141.31

Table 2: Samples of numerical results using FEM.

It is now possible to train a GMDH-type neural network to predict the output values $\hat{y}_i$ for any given input vector

$$\hat{y}_i = \hat{f}(x_{i1}, x_{i2}, x_{i3}, ..., x_{in}) \quad i = 1,2,...,n \tag{4}$$

Now the problem is to determine a GMDH-type neural network so that the square of difference between the actual output and the predicted one is minimized, so that:

$$\sum_{i=1}^{n} \left(\hat{y}_i - y_i\right)^2 \rightarrow Min \tag{5}$$

The general connection between input and output variables can be expressed by a complicated discrete form of the Volterra functional series in the form of:

$$y = a_0 + \sum_{i=1}^{n} a_i x_i + \sum_{i=1}^{n}\sum_{j=1}^{n} a_{ij} x_i x_j + \sum_{i=1}^{n}\sum_{j=1}^{n}\sum_{k=1}^{n} a_{ijk} x_i x_j x_k + ... \tag{6}$$

There are two main concepts involved within GMDH type neural networks design, namely the parametric and the structural identification problems. In this way, some works by Jamali et al. present a hybrid GA and singular value decomposition (SVD) method to optimally design such polynomial neural networks (Jamali et al., 2009). The methodology in these references has been successfully used in this paper to obtain the polynomial model of the thin-walled combined energy absorber crush behaviour with minimum training errors. The obtained GMDH-type polynomial models have been illustrated a very good prediction ability of the unforeseen data pairs during the training process.

6 RESULTS AND DISCUSSION

As is mentioned before, the relation between the first and second peak force and the energy absorption of the combined energy absorber with the geometrical variables like R, l, b, t was extracted by means of GMDH-type neural network. The input of the GMDH neural network would be the 192 random finite element analyses which were carried out for the training the GMDH neural network. Fifteen random analyses were selected for evaluating the capability of the GMDH neural network to predict the relation of the functions and the geometrical variables. For training the neural network, SVD hybrid and the evolutionary method are utilized. The very good behaviours of the GMDH-type neural network models for energy absorption have been also depicted in Figure 8 for both train and test data.

Figures 9, 11 and 13 show neural network structure for the modelling of objective functions and equations 7, 8 and 9 present according to these tree structures.

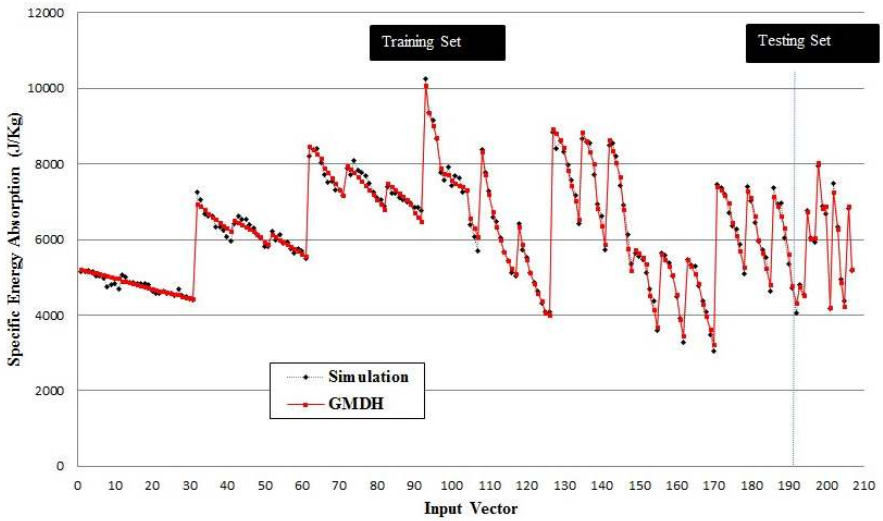


Figure 8: Comparison between finite element and GMDH model for the amount of Specific Energy Absorption.

Such behaviours have also been shown for peak crushing force for each of the training and testing data in Figures 10 and 12. It is obvious from these figures that the evolved GMDH-type neural network in terms of simple polynomial equations can successfully model and predict the output of testing data that have not been used during the training process.

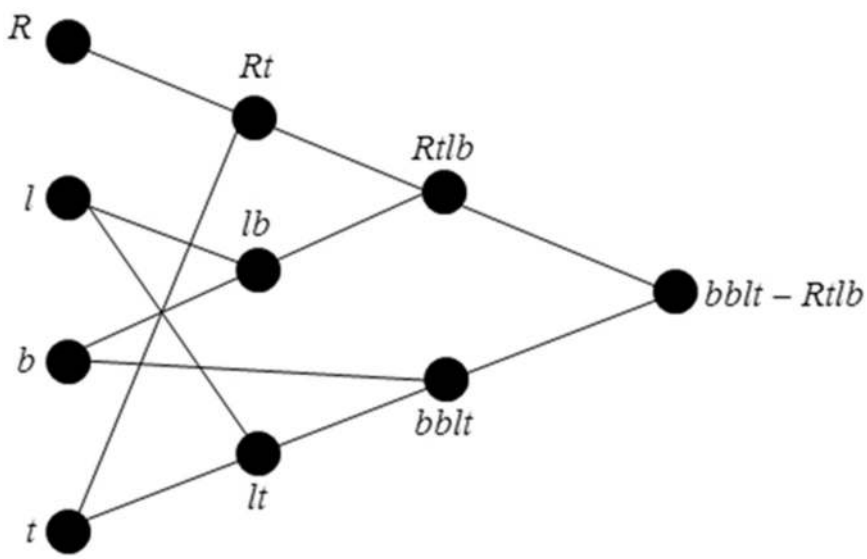


Figure 9: Neural network structure for modelling the Specific Energy Absorption.

The GMDH-type neural networks have been used for such training input–output data to find the polynomial model of energy absorption and peak crushing load with respect to their effective geometrical design variables.

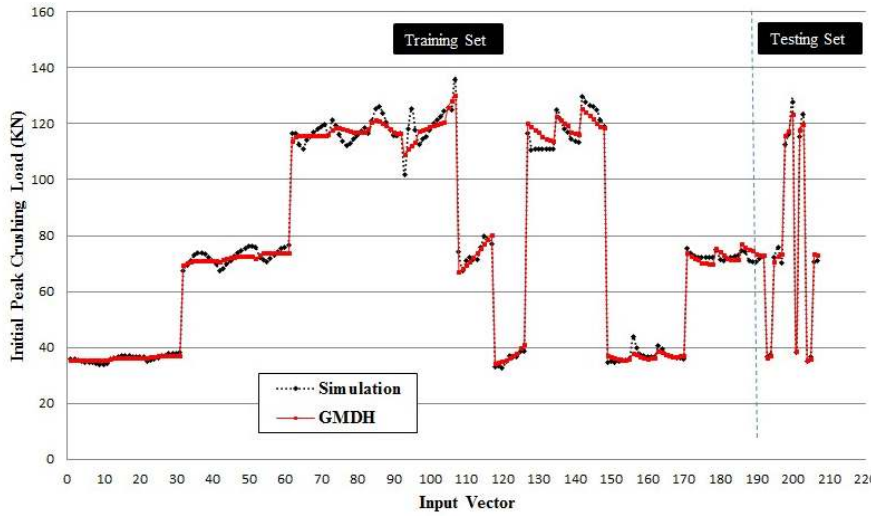


Figure 10: Comparison between finite element and GMDH model for Initial Peak Crushing Load.

In order to genetically design such GMDH-type neural network described in the previous section, a population of 30 individuals with a crossover probability (Pc) of 0.7 and mutation probability (Pm) of 0.07 has been used in 450 generations in which no further improvement has been achieved for such population size.

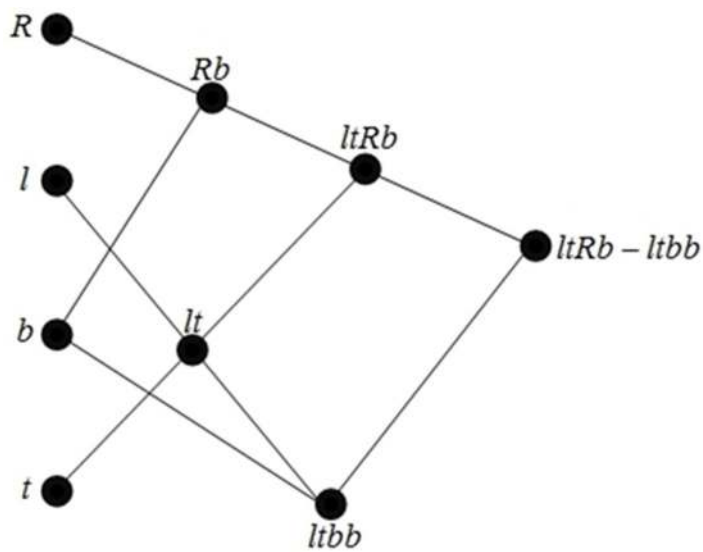


Figure 11: Neural network structure for modelling the Initial Peak Crushing Load.

The corresponding polynomial representations for specific energy absorption have been shown in equation 7.

$$
\begin{aligned}
Y_{lt} &= 2093.309 - 1.113l + 4066.670t - 0.004l^2 - 324.675t^2 - 1.156lt \\
Y_{Rt} &= 1081.843 + 1.396R + 4736.263t + 0.051R^2 - 342.407t^2 - 16.385Rt \\
Y_{lb} &= 10897.204 + 7.650l - 62.623b - 0.005l^2 + 0.271b^2 - 0.099lb \\
Y_{bblt} &= -0.298 - 28.853b + 2.042Y_{lt} + 0.219b^2 - 1.755\times10^{-5}Y_{lt}^{\ 2} - 0.008bY_{lt} \\
Y_{Rtlb} &= -6.692\times10^{-7} + 0.049Y_{Rt} - 0.044Y_{lb} + 2.531\times10^{-6}Y_{Rt}^{\ 2} + 9.676\times10^{-6}Y_{lb}^{\ 2} + 0.0001Y_{Rt}Y_{lb} \\
SEA &= 0.000134 + 1.022Y_{bblt} - 0.014Y_{Rtlb} - 0.000517Y_{bblt}^{\ 2} - 0.000372Y_{Rtlb}^{\ 2} + 0.000888Y_{bblt}Y_{Rtlb}
\end{aligned}
\tag{7}
$$

Similarly, the corresponding polynomial representations to model the initial and secondary peak crushing load have been depicted in equation 8 and 9.

$$
\begin{aligned}
Y_{lt} &= -9.701 - 0.003l + 30.242t + 1.726\times10^{-5}l^2 + 18.148t^2 - 0.010lt \\
Y_{Rb} &= 63.254 - 0.301R + 0.408b + 0.005R^2 - 1.179\times10^{-4}b^2 - 0.004Rb \\
Y_{ltRb} &= 221.559 - 0.293Y_{lt} - 5.149Y_{Rb} - 9.525\times10^{-6}Y_{lt}^{\ 2} + 0.029Y_{Rb}^{\ 2} + 0.017Y_{lt}Y_{Rb} \\
Y_{ltbb} &= 13.172 + 0.732Y_{lt} - 0.208b + 2.190\times10^{-5}Y_{lt}^{\ 2} + 7.613\times10^{-4}b^2 + 0.003Y_{lt}b \\
P_1 &= 0.773 - 1.297Y_{ltRb} + 2.272Y_{ltbb} - 0.158Y_{ltRb}^{\ 2} - 0.171Y_{ltbb}^{\ 2} + 0.329Y_{ltRb}Y_{ltbb}
\end{aligned}
\tag{8}
$$

$$
\begin{aligned}
Y_{Rt} &= 25.412 - 0.995R + 1.029t + 0.008R^2 + 5.621t^2 + 1.136Rt \\
Y_{lb} &= -2.491 + 0.286l + 1.718b - 5.396\times10^{-4}l^2 - 0.008b^2 - 7.507\times10^{-5}lb \\
Y_{Rb} &= 142.242 - 1.418R - 0.645b + 0.015R^2 - 3.233\times10^{-4}b^2 + 0.012Rb \\
Y_{Rtlb} &= -494.207 + 0.966Y_{Rt} + 9.118Y_{lb} - 6.563\times10^{-5}Y_{Rt}^{\ 2} - 0.042Y_{lb}^{\ 2} + 3.736\times10^{-4}Y_{Rt}Y_{lb} \\
Y_{Rbtt} &= -67.840 + 1.020Y_{Rb} - 9.131t - 0.004Y_{Rb}^{\ 2} + 5.529t^2 + 0.686Y_{Rb}t \\
P_2 &= 1.908 - 0.207Y_{Rtlb} + 1.221Y_{Rbtt} - 0.032Y_{Rtlb}^{\ 2} - 0.035Y_{Rbtt}^{\ 2} + 0.067Y_{Rtlb}Y_{Rbtt}
\end{aligned}
\tag{9}
$$

The models obtained in this section have been utilized for Pareto design of the combined energy absorber with geometrical parameters. Such a study may unveil some interesting and important optimal design principles that would not have been obtained without using this method.

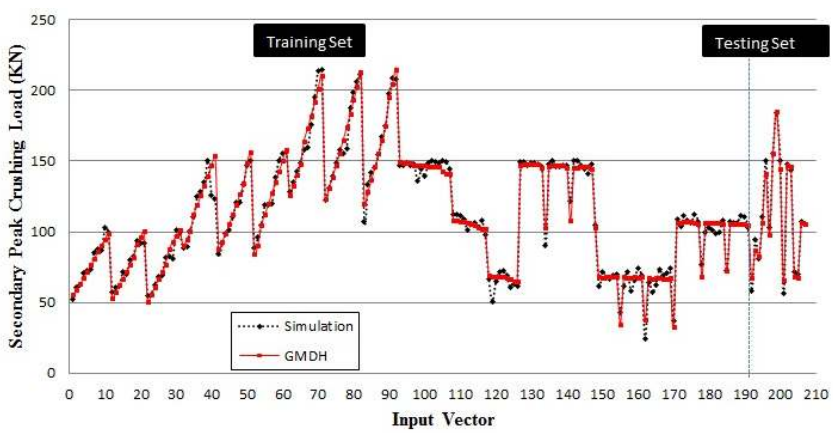


Figure 12: Comparison between finite element and GMDH model for Secondary Peak Crushing Load.

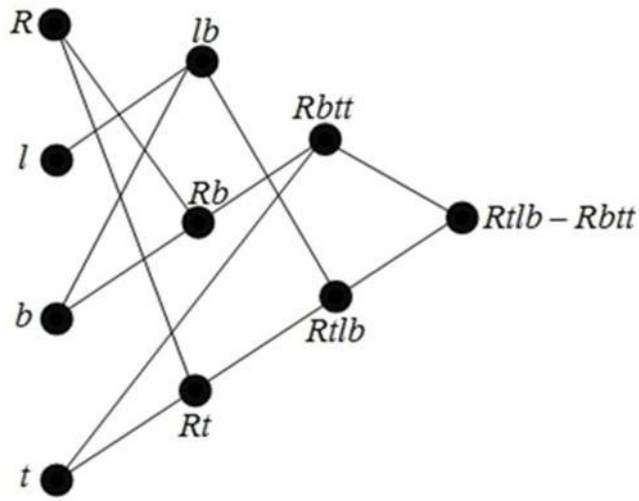


Figure 13: Neural network structure for modelling the Secondary Peak Crushing Load.

6.1 Multi-Objective Optimization

In this paper, for multi-objective optimization and Pareto graphs the modified NSGA-II Genetic Algorithm with the $\varepsilon - E$ lim *ination* diversity algorithm have been utilized (Atashkari et al., 2007). To obtain the evolutionary process of Pareto graphs multi-objective optimization has been accomplished by using the modified NSGA-II approach where a population size of 60 has been chosen in all runs with crossover probability (P_C) and mutation probability (P_M) as 0.7 and 0.07, respectively. The goal of this optimization is to maximize specific energy absorption simultaneously with the minimizing of primary and secondary peak crushing loads. This MOP can be formulated as follows:

$$\begin{cases} Maximize \rightarrow SEA \\ Minimize \rightarrow P_1 \ \ and \ \ P_2 \\ 1mm \le t \le 2mm,\ 60mm \le b \le 150mm \\ 43mm \le R \le 83mm,\ 58mm \le l \le 530mm \end{cases} \tag{10}$$

The Pareto graphs with respect to the objective functions have been plotted on different planes. In this case, none of Pareto points does not have the superiority of others and if any point is selected it will be in optimal conditions. It should be noted that there is a single set of individuals as a result of the three-objective optimization which have been shown in different planes of objective functions. Therefore, there are some points in each plane that may dominate others in the same plane. However, these individuals are all non-dominated when considering all tree objectives simultaneously. It is now desired to find a trade-off optimum design point from all non-dominated three-objective optimization processes with the compromising of all objective functions. This can be achieved by the nearest-to-ideal-point method and TOPSIS method (Atashkari et al., 2007) and (Lin and Yeh, 2012).

Figures 14, 15 and 16 show non-dominated points extracted from three-objective optimization which have been obtained from the above polynomials with respect to the objective functions in different planes. Points *"a"*, *"b"* and *"c"* have the highest specific energy absorption and the lowest

initial and secondary peak crushing load, respectively. Optimum design points, "*e*" and "*f*", are the points which have been obtained from the TOPSIS method and nearest-to-ideal-point method for objective function of specific energy absorption and secondary peak crushing load, respectively. Optimum design points, "*g*" and "*h*", are the points which have been obtained from the TOPSIS and nearest-to-ideal-point method for objective function of specific energy absorption and initial peak crushing load, respectively. The point *"d" has* been selected with both of the methods as the other optimal points of the objective function of the initial and secondary peak crushing load have been chosen. The dimensions of the optimum points have been presented in Table 3.

Optimum Design Point	$R(mm)$	$l(mm)$	$b(mm)$	$t(mm)$	$m(Kg)$	$SEA(J/Kg)$	$P_1(KN)$	$P_2(KN)$
d	43.00	75.2	.6020	1.01	1.11	6431.85	36.68	50.02
e	43.02	214.0	60.04	1.06	1.20	6871.85	38.49	64.94
f	43.02	217.5	60.51	1.43	1.62	8371.10	62.32	90.89
g	44.31	65.7	60.20	1.14	1.25	6832.45	44.51	53.61
h	43.47	82.8	60.24	1.47	1.61	8108.61	66.77	80.25

Table 3: Design parameters and results related to the optimum points.

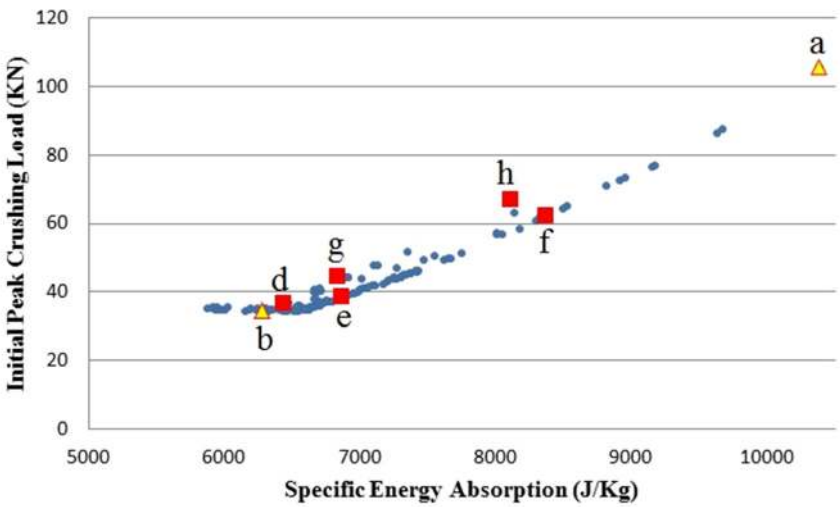


Figure 14: Pareto Graph: specific energy absorption to the Initial peak crushing load.

Figures 17 and 18 show the values of the design variables obtained from the three-objective optimization. The proposed optimal points have been illustrated on the graphs.

According to the figures it can be concluded that, because reducing the mass will be the main issue for the purpose of increasing the specific energy absorption; the radius of the circular cross section and the square width and thickness of structures should be small to reduce structural mass.

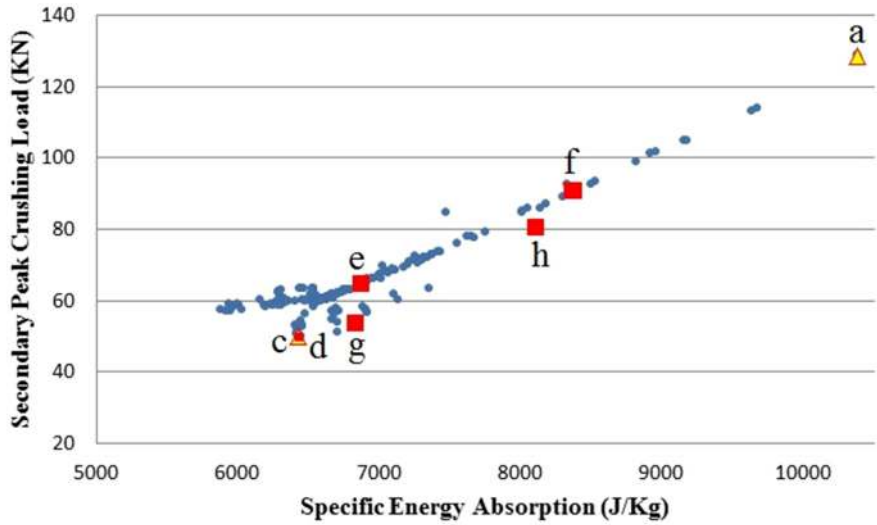


Figure 15: Pareto Graph: specific energy absorption to the secondary peak crushing load.

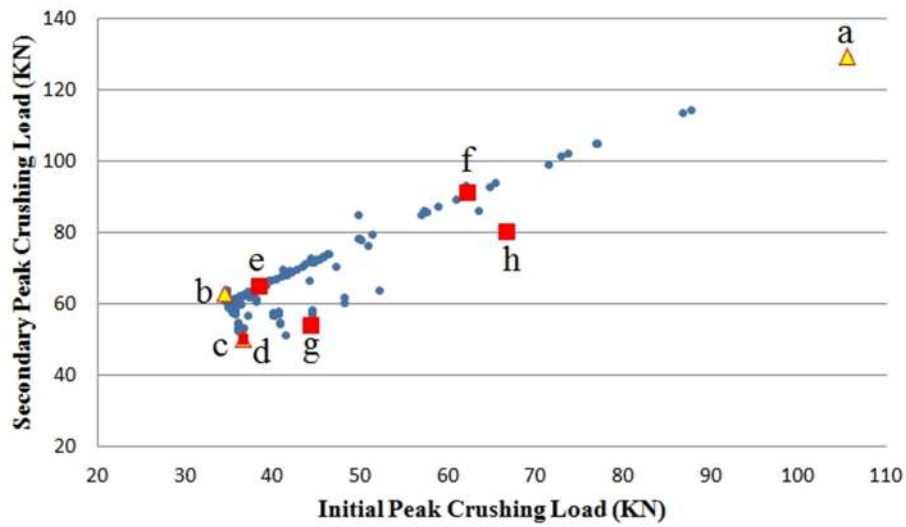


Figure 16: Pareto Graph: initial peak crushing load to the secondary peak crushing load.

The length of square section less than that of circular section will increase not only the energy absorption but also structure mass. As is demonstrated in Figures 17 and 18 the most optimal points are in range the of $43 \leq R \leq 45, 1 \leq t \leq 1.5$ and $60 \leq b \leq 70, 60 \leq l \leq 270$.

Furthermore the obtained optimal points are re-analyzed with the Abaqus/Explicit^{TM} finite element software.

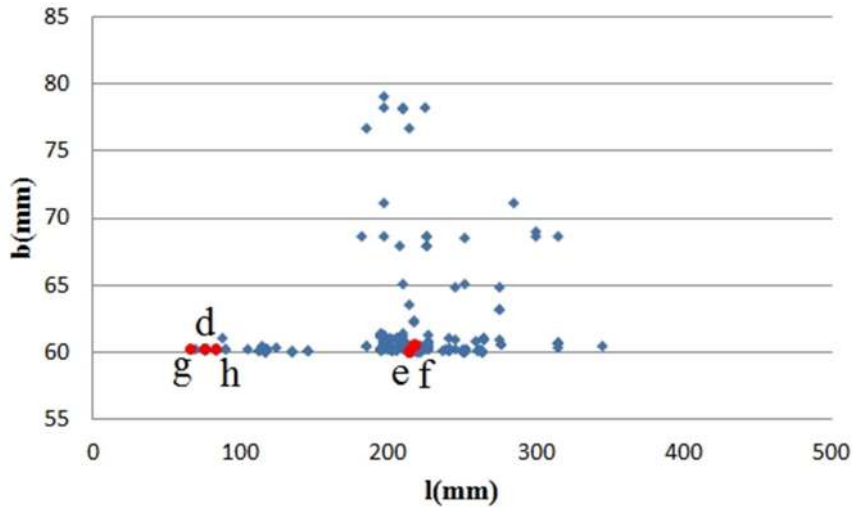


Figure 17: Design variables obtained from the three-objective optimization: *R,l,b,t*.

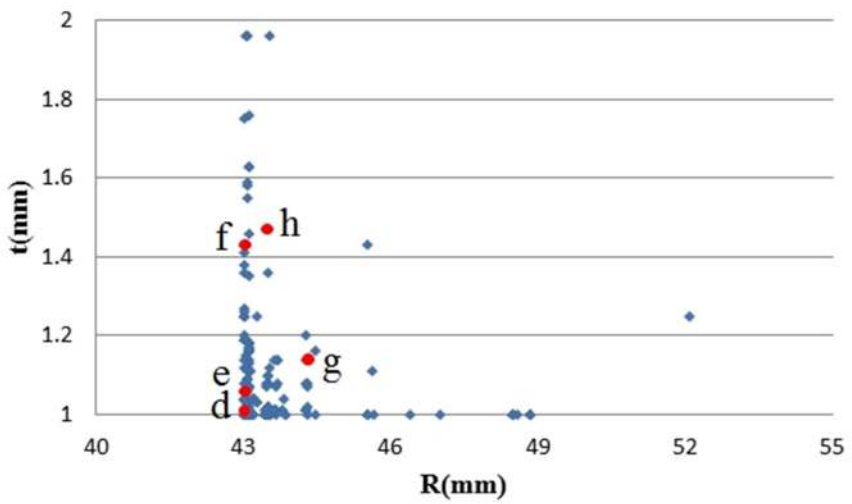


Figure 18: Design variables obtained from the three-objective optimization: *R,l,b,t*.

It should be noted that these optimum design points have not been included in the training and testing sets in the meta-modelling approach using GMDH-type neural network. The results of such FEM analysis have been illustrated in Table 4. The very close agreement of these results with those of numerical results using the GMDH model demonstrates the effectiveness of our approach in this paper. The shapes of deformation of the obtained design points (*d, f, g*) at the end displacement of 382 mm have been shown in Figure 19.

Optimum Design Point	d	e	f	g	h
$SEA(J/Kg)$	6746.1	7100.42	8641.48	7164.19	7420.53
Difference With GMDH (%)	+ 4.6	+ 3.2	+ 3.1	+ 4.6	-9.3
$P_1(KN)$	33.76	35.75	67.25	41.43	67.21
Difference With GMDH (%)	-8.6	- 7.7	+ 7.3	- 7.4	+ 0.6
$P_2(KN)$	45.63	59.51	83.30	59.04	86.12
Difference With GMDH (%)	-9.6	- 9.1	- 9.1	+ 9.2	+ 8.6

Table 4: Re-evaluation of the optimum points using FEM.

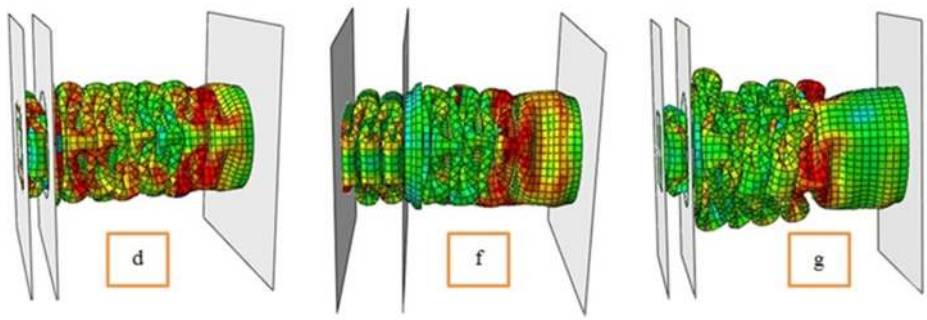


Figure 19: Deformation of the calculated optimal points.

For the square sections of these combined energy absorbers, taking the dimensions the same, leads to the equal energy absorption in the first part of the graph. With lower thickness of the *"d"* and *"g"* combined energy absorbers, thanks to the collapsing of the circular section which has been initiated in the displacement of 50mm, energy absorption of them would be equal to and even more than the *"f"* combined energy absorber until the displacement of 150mm. By beginning the collapse of the circular section of the *"f"* structure, the energy absorption of *"f"* would be in a rapid increase due to its higher thickness (Figures 20 and 21).

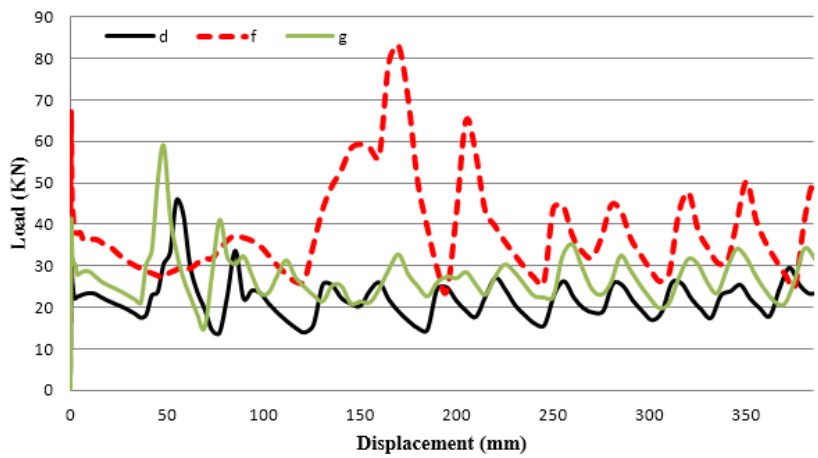


Figure 20: The crushing force–displacement curves of the optimum points.

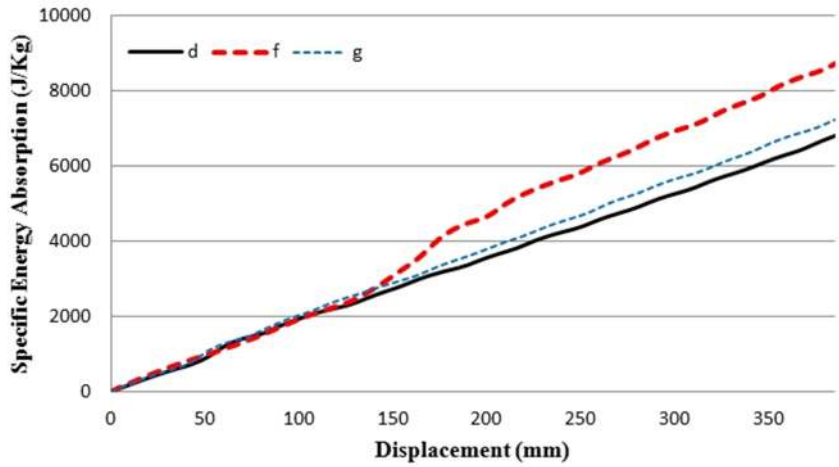


Figure 21: The specific energy absorption–displacement curves of the optimum points.

7 CONCLUSION

A new combined energy absorber has been developed and optimized in which the lower initial peak loads with higher energy absorption have been the main superiorities of this structure. The result of numerical finite element simulation has been validated by the experimental one. Moreover, the genetic algorithms have been utilized for optimal designing of generalised GMDH-type neural network models of combined energy absorber crush behaviour and for multi-objective Pareto-based optimisation of the structure. Three different polynomial relations for specific energy absorption, the initial peak crushing load and the secondary peak crushing load have been found by the developed GMDH-type neural network using some numerically input–output data from the FEM. The derived polynomial models have been then used in evolutionary multi-objective Pareto-based optimisation processes.

Such a combined application of GMDH neural network modelling of numerical and subsequent non-dominated Pareto optimisation process of the obtained meta-models has very promising in discovering useful and desirable design relationships.

References

Åström, K. J., Eykhoff, P. (1971). System identification—a survey. Automatica, 7(2): 123-162.

Atashkari, K., Nariman-Zadeh, N., Gölcü, M., Khalkhali, A., Jamali, A. (2007). Modelling and multi-objective optimization of a variable valve-timing spark-ignition engine using polynomial neural networks and evolutionary algorithms. Energy Conversion and Management, 48(3): 1029-1041.

Baroutaji, A., Gilchrist, M., Smyth, D., Olabi, A. (2015). Crush analysis and multi-objective optimization design for circular tube under quasi-static lateral loading. Thin-Walled Structures, 86 121-131.

Bi, J., Fang, H., Wang, Q., Ren, X. (2010). Modeling and optimization of foam-filled thin-walled columns for crashworthiness designs. Finite Elements in Analysis and Design, 46(9): 698-709.

Costas, M., Díaz, J., Romera, L., Hernández, S. (2014). A multi-objective surrogate-based optimization of the crashworthiness of a hybrid impact absorber. International Journal of Mechanical Sciences, 88 46-54.

Djamaluddin, F., Abdullah, S., Ariffin, A., Nopiah, Z. (2015). Optimization of foam-filled double circular tubes under axial and oblique impact loading conditions. Thin-Walled Structures, 87 1-11.

Farlow, S. J. (1984). Self-organizing methods in modeling: GMDH type algorithms (Vol. 54): CrC Press.

Ghafari-Namini, N., Ghasemnejad, H. (2012). Effect of natural stitched composites on the crashworthiness of box structures. Materials & design, 39 484-494.

Ivakhnenko, A. (1971). Polynomial theory of complex systems. Systems, Man and Cybernetics, IEEE Transactions on(4): 364-378.

Jamali, A., Nariman-Zadeh, N., Darvizeh, A., Masoumi, A., Hamrang, S. (2009). Multi-objective evolutionary optimization of polynomial neural networks for modelling and prediction of explosive cutting process. Engineering Applications of Artificial Intelligence, 22(4): 676-687.

Karagiozova, D., Alves, M., Jones, N. (2000). Inertia effects in axisymmetrically deformed cylindrical shells under axial impact. International Journal of Impact Engineering, 24(10): 1083-1115.

Kiasat, M., Najibi, A. (2008). Numerical Analysis of Crashworthiness of Circular and Square Tubes under Axial Crashing. ISME2008 May 14-16.

Li, Z., Yu, J., Guo, L. (2012). Deformation and energy absorption of aluminum foam-filled tubes subjected to oblique loading. International Journal of Mechanical Sciences, 54(1): 48-56.

Li, Z., Zheng, Z., Yu, J., Guo, L. (2013). Crashworthiness of foam-filled thin-walled circular tubes under dynamic bending. Materials & Design, 52 1058-1064.

Lin, Y.-K., Yeh, C.-T. (2012). Multi-objective optimization for stochastic computer networks using NSGA-II and TOPSIS. European Journal of Operational Research, 218(3): 735-746.

Mamalis, A., Johnson, W. (1983). The quasi-static crumpling of thin-walled circular cylinders and frusta under axial compression. International Journal of Mechanical Sciences, 25(9): 713-732.

Mamalis, A., Manolakos, D., Saigal, S., Viegelahn, G., Johnson, W. (1986). Extensible plastic collapse of thin-wall frusta as energy absorbers. International journal of mechanical sciences, 28(4): 219-229.

Qi, C., Yang, S., Dong, F. (2012). Crushing analysis and multiobjective crashworthiness optimization of tapered square tubes under oblique impact loading. Thin-Walled Structures, 59 103-119.

Qureshi, O. M., Bertocchi, E. (2012). Crash behavior of thin-Walled box beams with complex sinusoidal relief patterns. Thin-Walled Structures, 53 217-223.

Reid, S., Reddy, T., Gray, M. (1986). Static and dynamic axial crushing of foam-filled sheet metal tubes. International Journal of Mechanical Sciences, 28(5): 295-322.

Sanchez, E., Zadeh, L. A., Shibata, T. (1997). Genetic algorithms and fuzzy logic systems: World Scientific.

Sharifi, S., Shakeri, M., Fakhari, H. E., Bodaghi, M. (2015). Experimental investigation of bitubal circular energy absorbers under quasi-static axial load. Thin-Walled Structures, 89 42-53.

Shojaeefard, M. H., Najibi, A., Anbarloei, M., Yeganeh, M. (2014). Experimental and numerical crashworthiness investigation of combined circular and square sections. Journal of Mechanical Science and Technology, 28(3): 999-1006.

Tarlochan, F., Ramesh, S. (2012). Composite sandwich structures with nested inserts for energy absorption application. Composite Structures, 94(3): 904-916.

Tran, T., Hou, S., Han, X., Nguyen, N., Chau, M. (2014). Theoretical prediction and crashworthiness optimization of multi-cell square tubes under oblique impact loading. International Journal of Mechanical Sciences, 89 177-193.

Yin, H., Wen, G., Hou, S., Qing, Q. (2013). Multiobjective crashworthiness optimization of functionally lateral graded foam-filled tubes. Materials & Design, 44 414-428.